Resonance Contribution to Radiative Neutron Capture on Lithium-7

Fernando, Lakma; Higa, Renato; Rupak, Gautam

Published in:
Physical Review Letters

Resonance Contribution to Radiative Neutron Capture on Lithium-7

Lakma Fernando [a],* Renato Higa [b,c],† and Gautam Rupak [a]‡

[a] *Department of Physics & Astronomy and HPC^2 Center for Computational Sciences, Mississippi State University, Mississippi State, MS 39762, U.S.A.*

[b] *Kernfysisch Versneller Instituut, Theory Group, University of Groningen, 9747AA Groningen, The Netherlands*

[c] *Instituto de Física, Universidade de São Paulo, C.P. 66318, 05314-970, São Paulo, SP, Brazil*

Abstract

Using halo effective field theory, we provide a model-independent calculation of the radiative neutron capture on lithium-7 over an energy range where the contribution from the 3^+ resonance becomes important. One finds that a satisfactory description of the capture reaction, in the present single-particle approximation, suggests the use of a resonance width about three times larger than the experimental value. We also present power counting arguments that establish a hierarchy for electromagnetic one- and two-body currents.

PACS numbers: 25.40.Lw, 25.20.-x

Keywords: radiative capture, halo nuclei, effective field theory

* nkf22@msstate.edu

† higa@if.usp.br

‡ grupak@u.washington.edu

I. INTRODUCTION

The field of nuclear structure and reactions have witnessed continuous progress and renewal of interest with the advent of present and future facilities that are able to provide high-intensity beams of very unstable, rare isotopes —so-called exotic nuclei— whose physical properties are in the process of being uncovered. They populate areas in the nuclear chart far from the valley of stability, resembling more weakly-bound clusters rather than a tighter, shell-like structure. A subset in this exotic zoo comprises halo nuclei, systems formed by a tightly bound core nucleus surrounded by one or more loosely bound nucleons, with a slowly decreasing wave function tail that extends much farther than the effective core-nucleon interaction. Such extended and dilute configuration leads to threshold phenomena with consequences to low-energy nuclear astrophysics [1, 2].

An example of astrophysically relevant halo nucleus is boron-8, with dominant configuration of a beryllium-7 core loosely holding a proton by about a tenth of MeV. This nucleus plays a decisive role in our current understanding of neutrino physics. Underground detectors like SNO and Super-K are mainly sensitive to neutrinos released from the β-decay of ^{8}B in the Sun. The capture rate of a proton by beryllium-7 that produces boron-8, $^7\mathrm{Be}(p,\gamma)^8\mathrm{B}$, is crucial for determining the initial electron neutrino flux that eventually transmutes to other neutrino flavors on its way to detection. The reaction rate for conditions in the solar core sharply peaks around 20 keV, the Gamow peak, while experimental data remain above 100 keV. Measurements at lower energies are extremely difficult, mainly due to the Coulomb repulsion. The solar neutrino flux is therefore dependent on theoretical extrapolations of current data to lower energies. Available theoretical approaches [3–11] that use p-^{7}Be data alone, even with scattering information, are not well-constraining. The mirror system n-^{7}Li then becomes an important ingredient for benchmarking purposes —the Coulomb force between the initial particles is absent and more precise data at very low (sub-keV) energies are available. It also strongly constrains the $^7\mathrm{Be}(p,\gamma)^8\mathrm{B}$ if mirror symmetry, which ought to have its origins in the (accidental) isospin symmetry of QCD, is invoked. Besides, n-^{7}Li has its own astrophysical interest, bridging the path to the formation of heavier elements in inhomogeneous big-bang nucleosynthesis models [12].

The $^7\mathrm{Li}(n,\gamma)^8\mathrm{Li}$ cross section was calculated recently in effective field theory (EFT) for halo nuclei at low energy [13]. In this framework, the tight ^{7}Li core, inert and structureless

at leading order (LO), the loosely bound neutron, and the external soft photons are the relevant degrees of freedom. The main assumption of the approach is a single-particle approximation somewhat similar to models like Refs. [9–11, 14], where the valence nucleon interacts with the core via a Woods-Saxon potential. In halo EFT, however, a systematic and model-independent expansion of observables is achieved through the use of an expansion parameter —formed by the ratio of a soft scale Q, associated with the shallowness of the valence neutron, and a hard scale Λ, related to the tightness of the core. Moreover, the formalism guarantees unambiguous inclusion of electromagnetic interactions that preserve the required symmetry constraints, such as gauge invariance [13, 15]. In Ref. [13] only the leading E1 transition from initial s-wave continuum to the p-wave ^{8}Li ground state was considered. The authors found the poorly known p-wave effective range to be the leading source of uncertainty. In this work we extend the previous one in several directions, namely, we include explicitly the capture to the first excited state of ^{8}Li, the contribution from the low-lying p-wave resonance at ~ 0.22 MeV, and elaborate on the power counting for the two-body currents. With these extra ingredients, one sets the formalism that paves the way to handle the more weakly bound p-^{7}Be mirror system.

The paper is organized as follows. In Sec. II we develop the basic theory for the interactions necessary to calculate the capture reaction $^7\mathrm{Li}(n,\gamma)^8\mathrm{Li}$. We present the Lagrangian for elastic scattering in the s- and p-wave in the n+^{7}Li system and derive the one-body (magnetic moment) and two-body currents. We describe how the couplings in the EFT Lagrangian are constrained from available data on low-lying bound and resonance states. Results of our calculations are shown in Sec. III and compared with some available data and potential model calculations. We also present a brief discussion on higher-order terms and other degrees of freedom that becomes important at energies slightly above the ones considered here. Finally, we present our conclusions in Sec. IV. A more technical discussion about the power counting of two-body currents in the present approach is given in Appendix A.

II. FORMALISM

The low energy theory for $^7\mathrm{Li}(n,\gamma)^8\mathrm{Li}$ is constructed out of the spin-parity $\frac{1}{2}^+$ neutron and $\frac{3}{2}^-$ lithium-7 core. The final ^{8}Li nucleus contains the 2^+ and 1^+ ground and excited states in the bound spectrum. Very close to the n-^{7}Li threshold only the initial s-wave

states are relevant. As the energy increases around 200 keV a pronounced p-wave resonance in the initial state, identified as a 3^+ state, contributes. It is useful then to first list the possible initial and final channels for the reaction. Concentrating on just the s- and p-waves, we have in the spectroscopic notation $^{2S+1}L_J$: the initial s-wave states $^3S_1$ and $^5S_2$, the final p-wave channels $^3P_2$, $^5P_2$ for the ground state and $^3P_1$, $^5P_1$ channels for the excited state, and initial p-wave resonant state $^5P_3$. The 2^+ ground state of lithium-8 has the quantum numbers of both $^3P_2$ and $^5P_2$ states. It is, however, identified with the symmetric combination $|2^+\rangle \equiv (|^3P_2\rangle + |^5P_2\rangle)/\sqrt{2}$ [16]. The 1^+ excited state is primarily dominated by the antisymmetric combination $|1^+\rangle \equiv (|^5P_1\rangle - |^3P_1\rangle)/\sqrt{2}$ [7]. The 3^+ resonance can only belong to the $^5P_3$ channel in the present $n+^7$Li approach. The leading contribution to the capture reaction, which comes from the initial $^3S_1$ and $^5S_2$ states to the 2^+ ground state, proceeds through E1 transition due to electromagnetic selection rules. There is a small contribution from E1 capture to the excited 1^+ state with a branching ratio of 0.106 [17]. Finally, around 200 keV there is the M1 contribution from the 3^+ resonance to the 2^+ ground state.

In Ref. [13], the authors used the Clebsch-Gordan coefficient matrices Eq. (B6) to project the neutron $N(x)$, lithium-7 $C(x)$ fields onto the spin $S = 1$ and spin $S = 2$ channels as $N^T F_i C$ and $N^T Q_{ij} C$, respectively. We use the same formalism here to construct all the relevant initial and final states.

A. Interaction

The operators required for the calculation of the capture reaction $^7\mathrm{Li}(n,\gamma)^8\mathrm{Li}$ can be classified into three categories: (a) s-wave initial state elastic scattering $\mathcal{L}_s$, (b) p-wave elastic scattering to describe the 3^+ resonance, and analytically continued to describe the 2^+ ground and 1^+ excited states $\mathcal{L}_p$, and (c) two-body currents that are not related to the elastic channels $\mathcal{L}_{\rm EM} = O^M + O^L$.

The s-wave interaction Lagrangian is written as [13]

$$\mathcal{L}_s = g^{(1)}(N^T F_i C)^\dagger (N^T F_i C) + g^{(2)}(N^T Q_{ij} C)^\dagger (N^T Q_{ij} C) + \cdots , \tag{1}$$

where the "$\cdots$" represent higher derivative terms that are suppressed at low energy. At LO there is a single coupling $g^{(s)}$ in $^5S_2$ ($^3S_1$) spin channel that is fixed from the known s-wave

scattering length $a_0^{(2)} = -3.63 \pm 0.05$ fm ($a_0^{(1)} = 0.87 \pm 0.07$ fm) [18].

As discussed in the next subsection, the description of a low-energy p-wave bound/excited state or resonance requires two operators at LO [19, 20]. It is convenient to work in the dimer formalism, where the four-fermion contact interaction is replaced by the exchange of an auxiliary dimer field $\phi(x)$. The p-wave interaction Lagrangian then reads

$$\mathcal{L}_p^{(\eta)} = \phi_{[j]}^{(\eta)\dagger} \left[\left(i\partial_0 + \frac{\nabla^2}{2M} \right) + \Delta^{(\eta)} \right] \phi_{[j]}^{(\eta)} + h^{(\eta)} \left[\phi_{[j]}^{(\eta)} N^T P^{(\eta)} C + \text{H. c.} \right], \tag{2}$$

where $M = M_n + M_c$, neutron mass $M_n = 939.6$ MeV, ^{7}Li mass $M_c = 6535.4$ MeV and H.c. stands for Hermitian conjugate. $P_{[j]}^{(\eta)}$ are the projectors for the relevant p-wave channels: $^3P_1$, $^3P_2$, $^5P_1$, $^5P_2$, $^5P_3$ indicated by the index η and explicitly given in Appendix B. The subscript $[j]$ is a single, double or triple tensor indices as appropriate for $J = 1$, $J = 2$ and $J = 3$ state, respectively. The two EFT couplings $\Delta^{(\eta)}$, $h^{(\eta)}$ are proportional to the two required operators at LO and are determined from elastic scattering data as we discuss later.

For the capture through the 3^+ resonance state, we need the magnetic moment couplings

$$O^M = g_n \mu_N N^T \left(\frac{\boldsymbol{\sigma}}{2} \cdot \boldsymbol{B} \right) N + g_c \mu_N C^T \left(\boldsymbol{J} \cdot \boldsymbol{B} \right) C, \tag{3}$$

where $\boldsymbol{\sigma}$ are the Pauli matrices, $\boldsymbol{J}$ are the angular momentum matrices for spin-3/2 particle, $\boldsymbol{B} = \boldsymbol{\nabla} \times \boldsymbol{A}$ the magnetic field, μ_N the nuclear magneton, and $g_n \equiv 2\kappa_n$ and $g_c = 2\kappa_c/3$ are the neutron and the ^{7}Li gyromagnetic ratios, respectively. We take $\kappa_n = -1.91304$ and $\kappa_c = 3.256427$ as the corresponding magnetic moments [21]. In addition, there are contributions from two-body currents

$$O^L = i\mu_N \, L^{(2)} \phi_{ij}^{(^5P_2)\dagger} B_k \phi_{lmq}^{(^5P_3)} G_{ijklmq} + \mu_N \, L^{(1)} \phi_{ij}^{(^3P_2)\dagger} B_k \phi_{lmq}^{(^5P_3)} G_{ijklmq} + \text{H.c.}, \tag{4}$$

that contribute to M1 transition from initial $^5P_3$ state to final $^5P_2$ and $^3P_2$ states, respectively. The tensor G_{ijklmq} is defined in Appendix B. The two-body currents are allowed by symmetry so they contribute to the M1 capture. Further, the two-body couplings $L^{(1)}$, $L^{(2)}$ also regulate the divergences that appear in certain loop diagrams. The power counting for the different interactions will be presented in details in the following and in Appendix A.

B. EFT couplings

The couplings in Eqs. (1), (2) can be related to elastic scattering data in the s- and p-waves when available. Therefore, it is appropriate to match the field theory to the low-

energy amplitude written in terms of the effective range expansion (ERE). In principle, one could incorporate relativistic corrections in the EFT amplitude and go beyond the ERE [22]. However, this is not required at the low energies that we are interested in here. The two-body current couplings $L^{(\eta)}$ are not related to the elastic scattering data, and are thus determined from the capture data (see Sec. III).

The ERE elastic scattering amplitude in the ℓ-th partial wave is written as

$$i\mathcal{A}_\ell(p) = \frac{2\pi}{\mu}\frac{ip^{2\ell}}{p^{2\ell+1}\cot\delta_\ell - ip^{2\ell+1}} = \frac{2\pi}{\mu}\frac{ip^{2\ell}}{-1/a_\ell + \frac{1}{2}r_\ell p^2 + \frac{1}{2}t_\ell p^4 + \cdots - ip^{2\ell+1}}, \tag{5}$$

with reduced mass μ, and a_ℓ, r_ℓ, t_ℓ, etc., ERE parameters. Each term is assigned a momentum scaling, in general, given by dimensional analysis. Since the ERE parameters are associated with the short range (high momentum Λ) nuclear interaction, naively one would expect $a_\ell \sim \Lambda^{2\ell+1}$, $r_\ell \sim \Lambda^{2\ell-1}$, $t_\ell \sim \Lambda^{2\ell-3}$, and so on. At arbitrarily low momentum $p \sim Q$ one can expand the amplitude $\mathcal{A}_\ell$ in a Taylor series around $Q/\Lambda = 0$, a situation where the interaction is weak and perturbative. The more interesting situation arises when there are shallow bound or virtual states that one wishes to incorporate in the formalism. That implies a rearrangement of the perturbative series, which is only possible if at least one of the ERE parameters (usually the scattering length) has a different scaling than the one assumed by naive dimensional analysis. The s- and p-wave scattering amplitudes at LO then read [19, 20, 22, 23]

$$i\mathcal{A}_0(p) = \frac{2\pi}{\mu}\frac{i}{-1/a_0 - ip}\ , \tag{6}$$

$$i\mathcal{A}_1(p) = \frac{2\pi}{\mu}\frac{ip^2}{-1/a_1 + \frac{1}{2}r_1 p^2 - ip^3}\ . \tag{7}$$

For a shallow bound or virtual state in s-wave we set $1/a_0 \sim Q$, then only one single operator is needed at LO. For a shallow p-wave the situation is more subtle. First, only one particular fine-tuning of the scattering "length", $1/a_1 \sim Q^2\Lambda$, is enough to produce the shallow state [20]. However, not only one but two operators emerge at LO, since the effective "range" term $r_1 p^2/2 \sim Q^2\Lambda$ now scales equally as $1/a_1$ at momenta $p \sim Q$. Second, the unitarity term $ip^3 \sim Q^3$ is in principle of higher order. The p-wave amplitude $\mathcal{A}_1$ is then suppressed by Q/Λ relative to $\mathcal{A}_0$. However, for energies close to the resonant state there is a cancellation of the leading terms (kinematical fine-tuning [20, 24]) that makes $-1/a_1 + rp^2/2 \sim Q^3$ and promotes the unitarity term ip^3 to LO. In that region, the amplitudes (6) and (7) contribute at the same order.

The elastic scattering amplitude in EFT is calculated from the interactions in Eqs. (1), (2) as shown in Fig. 1. We get for the s-wave amplitude

$$
\begin{aligned}
i\mathcal{A}_0^{(\eta)}(p) &= \frac{ig^{(\eta)}}{1 - ig^{(\eta)} f_0(p)}, \\
f_0(p) &= -i2\mu \left(\frac{\lambda}{2}\right)^{4-D} \int \frac{d^{D-1}\boldsymbol{q}}{(2\pi)^{D-1}} \frac{1}{q^2 - p^2 - i0^+} = -\frac{i\mu}{2\pi}(\lambda + ip),
\end{aligned}
\tag{8}
$$

with renormalization scale λ. Comparing Eqs. (8) and (6) we find [22, 23]

$$
g^{(\eta)}(\lambda) = \frac{2\pi}{\mu} \frac{1}{\lambda - 1/a_0^{(\eta)}},
\tag{9}
$$

where $\eta = 1, 2$ correspond to spin channels ${}^3S_1$, ${}^5S_2$, respectively.

For the p-wave amplitude we have from Fig. 1

$$
i\mathcal{A}_1^{(\eta)} = -[h^{(\eta)}]^2 \frac{p^2}{\mu^2} iD^{(\eta)}(p^2/2\mu, 0) = \frac{2\pi}{\mu} \frac{ip^2}{-\frac{2\pi\mu\Delta^{(\eta)}}{[h^{(\eta)}]^2} - \frac{\pi\lambda^3}{2} - \left(\frac{3\lambda}{2} + \frac{\pi}{[h^{(\eta)}]^2}\right) p^2 - ip^3},
\tag{10}
$$

using the full dimer propagator

$$
\begin{aligned}
iD^{(\kappa)}(p_0, \boldsymbol{p}) &= \frac{i}{\Delta^{(\kappa)} - \frac{1}{2\mu}\zeta^2 + \frac{2h^{(\kappa)\,2}}{\mu} f_1(p_0, \boldsymbol{p})}, \\
f_1(p_0, \boldsymbol{p}) &= \frac{1}{4\pi}\left(\zeta^3 - \frac{3}{2}\zeta^2\lambda + \frac{\pi}{2}\lambda^3\right),
\end{aligned}
\tag{11}
$$

where $\zeta = \sqrt{-2\mu p_0 + \mu p^2/M - i0^+}$. Matching the EFT amplitude to the p-wave ERE expansion determines the coupling pair ($\Delta^{(\kappa)}$, $h^{(\kappa)}$). As in the s-wave, comparing Eqs. (10) and (7) yields

$$
\begin{aligned}
-\frac{2\pi\mu\Delta^{(\eta)}}{[h^{(\eta)}]^2} - \frac{\pi}{2}\lambda^3 &= -1/a_1^{(\eta)}, \\
-\frac{3}{2}\lambda - \frac{\pi}{[h^{(\eta)}]^2} &= \frac{1}{2} r_1^{(\eta)}.
\end{aligned}
\tag{12}
$$

The index η identifies the relevant p-wave channels outlined earlier. The EFT couplings $\Delta^{(\eta)}$, $h^{(\eta)}$ are therefore fixed in terms of the ERE parameters $a_1^{(\eta)}$, $r_1^{(\eta)}$ and the renormalization scale λ.

In the ${}^5P_3$ resonance channel we call $\eta = 3$ and directly use the relations in Eq. (12). The parameters $a_1^{(3)}$ and $r_1^{(3)}$ are related to the known resonance position and width, as shown in Sec. II C.

For the bound channels 1^+, 2^+, we follow the procedure used in Ref. [13]. It is more convenient to work directly with the location of the pole in the dimer propagator at the

binding momentum $\gamma^{(\eta)}$ and its residue $\mathcal{Z}^{(\eta)}$. The latter is the wave function renormalization constant calculated using Eqs. (11), (12) as

$$\begin{aligned}[\mathcal{Z}^{(\eta)}]^{-1} =& \frac{\partial}{\partial p_0}[D^{(\eta)}(p_0, \boldsymbol{p})]^{-1}\big|_{p_0=\boldsymbol{p}^2/(2M)-B^{(\eta)}}, \\ \mathcal{Z}^{(\eta)} =& -\frac{2\pi}{[h^{(\eta)}]^2}\frac{1}{3\gamma^{(\eta)}+r_1^{(\eta)}},\end{aligned} \tag{13}$$

where $B^{(\eta)} = [\gamma^{(\eta)}]^2/(2\mu)$ is the binding energy. The ${}^3P_2$ and ${}^5P_2$ channels in 2^+ share a common binding momentum $\gamma^{(2^+)} \approx 57.8$ MeV. Moreover, the capture cross section is not independently sensitive to the effective range parameter r_1 in these two spin channels [13]. For this reason we use a common effective range parameter $r_1^{(2^+)}$. This coincidentally gives the observed ratio 0.82 of spin channel $S = 2$ relative to the total E1 capture to the ground state at threshold [25]. We make a similar simplifying assumption for the 1^+ state and use a common effective range parameter $r_1^{(1^+)}$ for both spin channels ${}^3P_1$, ${}^5P_1$. In the final cross section only the combinations

$$\begin{aligned}[h^{(2^+)}]^2\mathcal{Z}^{(2^+)} &= -\frac{2\pi}{3\gamma^{(2^+)}+r_1^{(2^+)}}, \\ [h^{(1^+)}]^2\mathcal{Z}^{(1^+)} &= -\frac{2\pi}{3\gamma^{(1^+)}+r_1^{(1^+)}},\end{aligned} \tag{14}$$

contribute to the 2^+ and 1^+ states, respectively. In Ref. [13], $r_1^{(2^+)} \approx -1.55$ fm^{-1} from a fit to low energy data from Ref. [26]. $\gamma^{(1^+)} \approx 41.6$ MeV from the known 1^+ excited state energy. We will determine $r_1^{(2^+)}$ and $r_1^{(1^+)}$ in this work from the known E1 thermal capture rates to the 2^+ and 1^+ states [17], respectively.

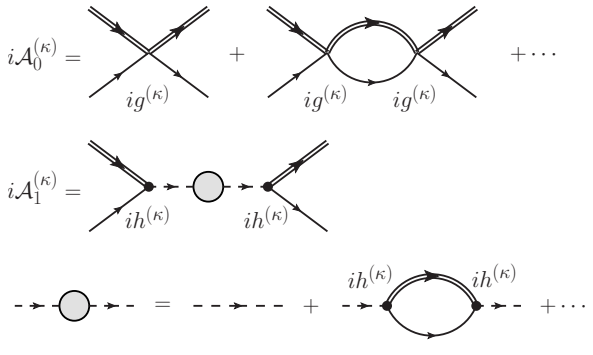

FIG. 1. Initial s-wave $\mathcal{A}_0^{(\kappa)}$ and p-wave $\mathcal{A}_1^{(\kappa)}$ elastic scattering amplitudes. Double line is the ^{7}Li propagator, single line the neutron propagator, dashed line the bare dimer propagator.

C. Resonance parameters

The p-wave EFT couplings for the 3^+ ($^5P_3$) state can be related to the ERE scattering parameters $a_1^{(3)}$ and $r_1^{(3)}$ through Eq (12). Since these ERE parameters are not known we first determine them from the known resonance energy and width. At very low momentum, the phase shift $\delta(p)$ in this channel vanishes due to the centrifugal barrier. Near the resonance, $\delta(p)$ increases rapidly through $\pi/2$ from below. Thus, $\cot\delta(p)$ has to go through zero from above, *i.e.*, it has a negative slope. We write these conditions as [27]

$$\begin{aligned} \cot\delta\Big|_{E=E_r} &= 0, \quad \text{and} \\ \frac{d}{dE}\cot\delta\Big|_{E=E_r} &= -c < 0, \end{aligned} \tag{15}$$

such that $c > 0$. Near the resonance

$$\begin{aligned} \cot\delta(E) \approx& \cot\delta(E_r) + (E-E_r)\cot'\delta(E_r) = -(E-E_r)c, \\ \mathcal{A}(p) =& \frac{2\pi}{\mu}\frac{1}{p\cot\delta - ip} \approx \frac{2\pi}{\mu p}\frac{-\Gamma_r/2}{(E-E_r)+i\Gamma_r/2}, \end{aligned} \tag{16}$$

and we recover the Breit-Wigner form, identifying $c \equiv 2/\Gamma_r$. The resonance position and width can be related to the ERE scattering parameters. In the center-of-mass (c.m.) frame we define $p_r^2 \equiv 2\mu E_r$, then

$$\begin{aligned} p^3\cot\delta = -\frac{1}{a_1^{(3)}} + \frac{r_1^{(3)}p^2}{2} \Rightarrow \cot\delta(p_r) = -\frac{1}{a_1^{(3)}p_r^3} + \frac{r_1^{(3)}}{2p_r} = 0, \quad \text{and} \\ \frac{d}{dE}\cot\delta(E_r) = \frac{\mu}{p_r}\frac{d}{dp_r}\cot\delta(p_r) = -2/\Gamma_r \Rightarrow \frac{3}{a_1^{(3)}p_r^4} - \frac{r_1^{(3)}}{2p_r^2} = -\frac{2p_r}{\mu\Gamma_r}. \end{aligned} \tag{17}$$

For the resonance momentum and width one gets (see also Refs. [28, 29])

$$p_r^2 = \frac{2}{a_1^{(3)}r_1^{(3)}}\,, \qquad \text{and} \qquad \Gamma_r = -\frac{2p_r^3}{\mu r_1^{(3)}}\,. \tag{18}$$

Solving these equations we find

$$a_1^{(3)} = -\frac{\mu\Gamma_r}{p_r^5}, \quad \text{and} \quad r_1^{(3)} = -\frac{2p_r^3}{\mu\Gamma_r}. \tag{19}$$

We choose $p_r = +\sqrt{2\mu E_r}$ so that $(a_1^{(3)}, r_1^{(3)})$ are negative to be consistent with the Wigner bound [30]. If we take the experimental central values for $E_r = 0.222$ MeV and $\Gamma_r = 0.031$ MeV in the c.m. frame we find $(|1/a_1^{(3)}|^{1/3}, r_1^{(3)}) = (46.38, -547.1)$ MeV, and from Eq (12) we are able to determine the EFT couplings.

To test the robustness of the above procedure we generate "synthetic data" for the resonance phase shifts from a known nuclear interaction. We take a single-particle potential given by the Woods-Saxon form [11],

$$V(r) = -v_0 \left[1 + \exp\left(\frac{r - R_c}{a_c}\right)\right]^{-1} + \frac{1}{2}\frac{v_{so}}{r}\frac{d}{dr}\left[1 + \exp\left(\frac{r - R_c}{a_c}\right)\right]^{-1}, \tag{20}$$

where the 1/2 factor in the second term comes from the expectation value of the single-particle spin-orbit operator in the 3^+ channel. We use natural units with $\hbar = 1 = c$. In a study by Tombrello [9], the central potential with a depth $v_0 = 26.42$ MeV, spin-orbit $v_{so} = 0$, range $R_c = 2.95$ fm and diffusiveness $a_c = 0.52$ fm was used to reproduce the resonance energy. A more recent work from Huang et al. [11] uses $v_0 = 34.93$ MeV, spin-orbit potential depth $v_{so} = 10$ MeV, $R_c = 2.391$ fm, and $a_c = 0.65$ fm. The two sets of parameters produce nearly identical phase shifts, Fig.2. Plugging Huang's synthetic data into Eq. (15) generates $E_r = 0.228$ MeV and $\Gamma_r = 0.115$ MeV. From Eq. (19) one gets $(|1/a_1^{(3)}|^{1/3}, r_1^{(3)}) = (30.69, -154.3)$ MeV, which are then used as input to the EFT curve shown in Fig.2. Alternatively, one can extract directly the ERE parameters from the low-energy behavior of the phase shifts: $(|1/a_1^{(3)}|^{1/3}, r_1^{(3)}) = (31.02, -157.6)$ MeV and $(|1/a_1^{(3)}|^{1/3}, r_1^{(3)}) = (30.84, -158.9)$ MeV in the case of Tombrello and Huang's parameters, respectively. We also show the Breit-Wigner curve using the extracted resonance parameters. We see that the procedure outlined allows EFT to reproduce well the synthetic data at low energy.

We further note that the potential model parameters chosen give a resonance width that is about three times larger than the experimental value. As we discuss in Sec. III, it does impact the shape of the M1 curve in the capture reaction. To fit the resonance width to experimental data would require tuning yet another parameter (besides the potential depth) in the Woods-Saxon potential. In the EFT language, two operators are required to describe a shallow p-wave resonance at LO. The corresponding couplings $(\Delta^{(3)}, h^{(3)})$ are directly related to two experimental data: E_r and Γ_r.

III. CAPTURE CROSS SECTION

The $^7\mathrm{Li}(n,\gamma)^8\mathrm{Li}$ capture from $E = 0$ to about 0.15 MeV total c.m. energy is almost entirely given by the E1 transition from initial s-waves. The dominant contribution goes

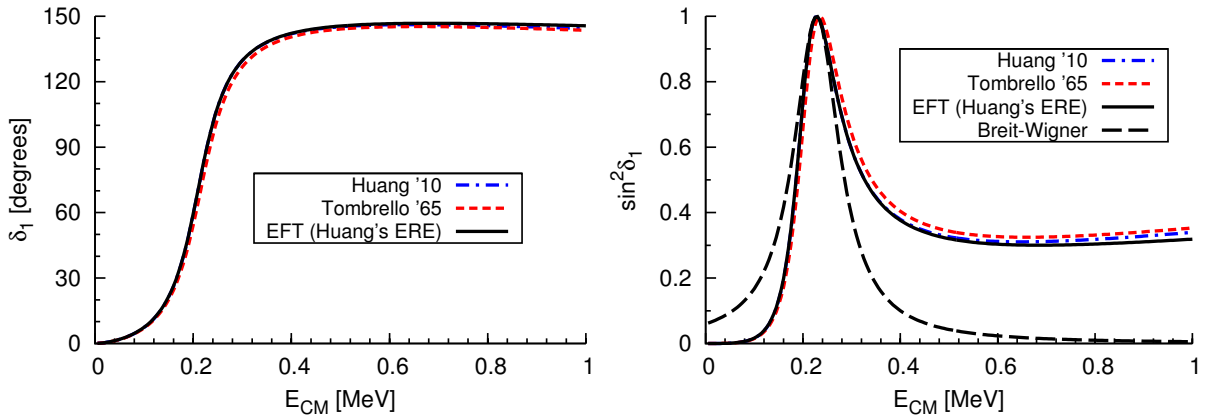

FIG. 2. ${}^5P_3$ phase shifts. Blue dot-dashed curve using Huang's [11] Woods-Saxon parameters, red dashed curve using Tombrello's [9] parameters, black solid curve EFT fitted to Huang's "synthetic data", black long-dashed curve Breit-Wigner form.

directly to the 2^+ ground state, with a small fraction (about 10%) going to the 1^+ excited state. In a recent work [13] the former was calculated explicitly, but the later was only taken into account implicitly with the use of the experimental branching ratio. Around $E \approx 200$ keV the 3^+ resonance enhances the cross section through an M1 transition to the ground state. In this section we derive expressions for these three low-energy mechanisms and compare our results with potential model calculations and few available experimental data.

The ${}^7\mathrm{Li}(n,\gamma){}^8\mathrm{Li}$ cross section is calculated in the c.m. frame with $\boldsymbol{p}$ ($\boldsymbol{k}$) the core (photon) momentum and $\hat{\boldsymbol{k}} \cdot \hat{\boldsymbol{p}} = \cos\theta$. The incoming momentum p as well as the binding momenta for the ground and excited states $\gamma^{(\eta)}$ are assumed to be of the order of the low-energy scale, *i.e.*, $p \sim \gamma^{(\eta)} \sim Q$. The photon at LO has $|\boldsymbol{k}| = k_0 \approx (p^2 + [\gamma^{(\eta)}]^2)/(2\mu)$ and the Mandelstam variable $s \approx (M_n + M_c)^2 = M^2$. The c.m. differential cross section is

$$\frac{d\sigma}{d\phi d\cos\theta} = \frac{1}{64\pi^2 s}\frac{|\boldsymbol{k}|}{|\boldsymbol{p}|}|\mathcal{M}|^2 \approx \frac{1}{64\pi^2 M^2}\frac{p^2 + [\gamma^{(\eta)}]^2}{2\mu p}|\mathcal{M}|^2, \tag{21}$$

where $\gamma^{(2^+)} \approx 57.8$ MeV and $\gamma^{(1^+)} \approx 41.6$ MeV for the 2^+ and 1^+ final states, respectively.

The E1 capture to the ground state at LO proceeds through the diagrams in Fig. 3. The photons are minimally coupled to the ${}^7\mathrm{Li}$ nucleus by gauging the core derivatives $\boldsymbol{\nabla}_C \to \boldsymbol{\nabla}_C + ieZ_c\boldsymbol{A}$ with $Z_c = 3$ the core charge. We quote the final result for capture to the ${}^5P_2$

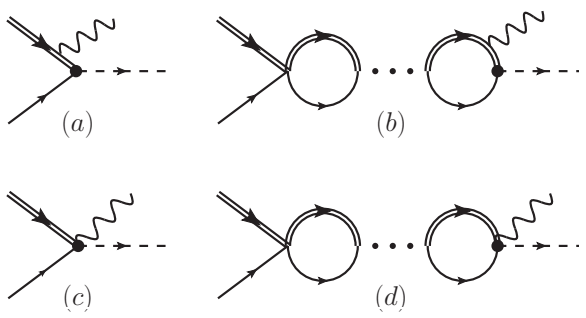

FIG. 3. Capture reactions $^7\mathrm{Li}(n,\gamma)^8\mathrm{Li}$. Wavy lines represent photons. "$\cdots$" represents initial state s-wave interaction.

state from Ref. [13] here for completeness:

$$\begin{aligned}\left|\mathcal{M}_{\mathrm{E1}}^{(^5P_2)}\right|^2 &= 5\left(\frac{Z_c M_n}{M}\right)^2 \frac{64\pi\alpha M^2\left|h^{(2^+)}\sqrt{\mathcal{Z}^{(2^+)}}\right|^2}{\mu} \\ &\times\left[|1+X|^2-\frac{p^2\sin^2\theta}{p^2+[\gamma^{(2^+)}]^2}\left(\frac{2[\gamma^{(2^+)}]^2}{p^2+[\gamma^{(2^+)}]^2}+X+X^*\right)\right], \qquad (22)\\ X &= \frac{1}{-1/a_0^{(2)}-ip}\left[\frac{2}{3}\frac{[\gamma^{(2^+)}]^3-ip^3}{[\gamma^{(2^+)}]^2+p^2}+ip\right],\end{aligned}$$

with $\alpha = e^2/(4\pi)$. The amplitude $\left|\mathcal{M}_{\mathrm{E1}}^{(^3P_2)}\right|$ is obtained from the above by replacing $a_0^{(2)} \to a_0^{(1)}$. The E1 transition to the 2^+ ground state is written as

$$\frac{d\sigma_{\mathrm{E1}}^{(2^+)}}{d\cos\theta} = \frac{1}{32\pi M^2}\frac{p^2+[\gamma^{(2^+)}]^2}{2\mu p}\frac{1}{8}\frac{\left|\mathcal{M}_{\mathrm{E1}}^{(^5P_2)}\right|^2+\left|\mathcal{M}_{\mathrm{E1}}^{(^3P_2)}\right|^2}{2}, \qquad (23)$$

taking the ^{8}Li ground state $|2^+\rangle$ as the symmetric combination of final states. The total cross section $\sigma(p)$ is obtained from a straightforward integration over the angle θ. We have used a common effective range parameter $r_1^{(2^+)}$ in $\mathcal{Z}^{(2^+)}$ as explained earlier, see Ref. [13] for details. Fitting to the thermal cross section $\sigma^{(2^+)} = 40.56$ mb [17] gives $r_1^{(2^+)} = -1.47$ fm^{-1}, which is close to the $r_1^{(2^+)} = -1.55$ fm^{-1} value one gets using the data from Ref [26]. In this work we will use the value obtained from the thermal capture.

The E1 capture cross section to the 1^+ excited state, $\sigma_{\mathrm{E1}}^{(1^+)}$, comprises the same set of diagrams in Fig. 3 except the final state dimer, which is in the 1^+ state. The sum over the

final polarization states gives an overall factor of 3 instead of 5. Therefore we have

$$\left|\mathcal{M}_{\rm E1}^{(^5P_1)}\right|^2 = 3\left(\frac{Z_c M_n}{M}\right)^2 \frac{64\pi\alpha M^2 \left|h^{(1^+)}\sqrt{\mathcal{Z}^{(1^+)}}\right|^2}{\mu} \times\left[|1+Y|^2 - \frac{p^2\sin^2\theta}{p^2+[\gamma^{(1^+)}]^2}\left(\frac{2[\gamma^{(1^+)}]^2}{p^2+[\gamma^{(1^+)}]^2}+Y+Y^*\right)\right], \tag{24}$$

$$Y = \frac{1}{-1/a_0^{(2)}-ip}\left[\frac{2}{3}\frac{[\gamma^{(1^+)}]^3-ip^3}{p^2+[\gamma^{(1^+)}]^2}+ip\right],$$

$$\frac{d\sigma_{\rm E1}^{(1^+)}}{d\cos\theta} = \frac{1}{32\pi M^2}\frac{p^2+[\gamma^{(1^+)}]^2}{2\mu p}\frac{1}{8}\frac{\left|\mathcal{M}_{\rm E1}^{(^5P_1)}\right|^2+\left|\mathcal{M}_{\rm E1}^{(^3P_1)}\right|^2}{2}, \tag{25}$$

where we made the replacements $[h^{(2^+)}]^2\mathcal{Z}^{(2^+)} \to [h^{(1^+)}]^2\mathcal{Z}^{(1^+)}$, $\gamma^{(2^+)} \to \gamma^{(1^+)}$ in Eqs. (24,25). The $|1^+\rangle$ state is considered the anti-symmetric combination of the final states. As in the 2^+ case, the amplitude in the other channel spin $\left|\mathcal{M}_{\rm E1}^{(^3P_1)}\right|$ is derived from $a_0^{(2)} \to a_0^{(1)}$, with a common effective range parameter $r_1^{(1^+)}$. From the thermal capture rate $\sigma^{(1^+)} = 4.80$ mb to the 1^+ state we get $r_1^{(1^+)} \approx -1.93$ fm^{-1}. The E1 capture cross section to the ground and excited state is shown in Fig. 4. We also show the potential model results for comparison. The leading uncertainty in potential model results seems to be associated with the poorly known effective range $r_1^{(2^+)}$ that we determine from the thermal capture rate. We also notice that the data set that we call ImhofB is more consistent with the $1/v$ behavior suggested by the Blackmon [26] and Lynn [17] data than ImhofA.

Next, we consider the M1 capture cross section. It proceeds through an initial p-wave state, and therefore, suppressed at low energies. In contrast, the E1 capture takes place via initial s-wave states and displays the known $1/p$ enhancement at low momentum. However, the presence of the 3^+ resonance enhances the M1 contribution around the resonance energy, making it comparable to E1. In Fig. 5 we show the diagrams that make the leading contributions to the M1 capture. The first two involve the neutron and core magnetic moment couplings, and contribute to both $^5P_2$ and $^3P_2$ final states. In the third one the magnetic photon couples to the charged ^{7}Li core "in flight" or, in a more classical picture, to the electromagnetic current generated by the orbital motion of the charged ^{7}Li core. It arises from minimal photon coupling and contributes only to the $^5P_2$ final state. The last diagram contains two-body currents in the respective $^5P_2$ and $^3P_2$ channels. Naively, counting only factors of Q/Λ, the contributions from two-body currents seem to be more important than

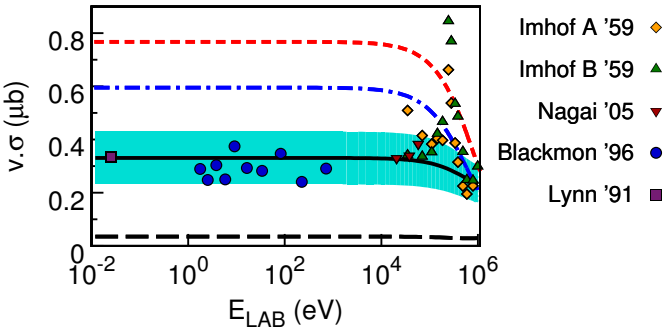

FIG. 4. Black long-dashed and solid curves are the EFT results for the E1 capture to the excited state and the total E1 capture, respectively. The shaded area shows the estimated 30% EFT errors in the latter. The results of the potential model code CDXS+ [31] using parameters from Ref. [10] and Ref. [9] are given respectively by the blue dot-dashed and red dashed curves. The experimental points are from Refs. [17, 26, 32, 33].

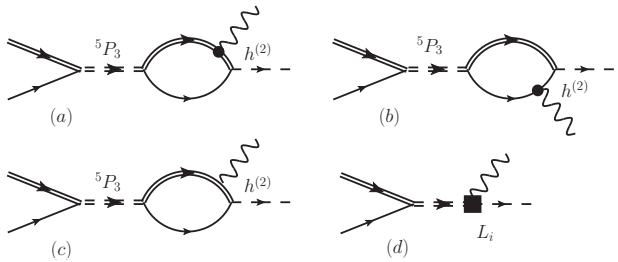

FIG. 5. The photon is coupled through the magnetic moment to the neutron (single solid line) and ^{7}Li nucleus (double solid line). Single dashed line is the ground state ^{8}Li 2^+ dressed dimer, double dashed line is the ^{8}Li 3^+ resonance dressed dimer.

the ones from the magnetic moments. We will come back to this point in the following.

Evaluation of these diagrams in the final $^5P_2$ channel yields

$$i\mathcal{M}_{\rm M1}^{(^5P_2)} = \epsilon_{abc}\varepsilon_{ij}^*\varepsilon_c^{(\gamma)*}G_{ijalmq}p_q k_b\, h^{(2^+)}\sqrt{2M\mathcal{Z}^{(2^+)}}\,\mu_N\left[-\frac{[h^{(3)}]^2}{2\pi\mu}D^{(3)}(p^2/2\mu,0)\right]\sqrt{3}$$
$$\times\, U_N^T(-\boldsymbol{p})Q_{lm}U_C(\boldsymbol{p})\left[\sqrt{\frac{3}{2}}\left(\frac{3}{2}g_c+\frac{1}{2}g_n+\frac{2\mu Z_c M_n}{M_c^2}\right)I(p;\lambda)-\frac{2\pi L^{(2)}}{h^{(3)}h^{(2^+)}}\right], \qquad (26)$$

with

$$I(p;\lambda)=\frac{2}{3}\frac{[\gamma^{(2^+)}]^3-ip^3}{[\gamma^{(2^+)}]^2+p^2}-\lambda. \qquad (27)$$

The various tensors above are defined in Appendix B. For the ${}^3P_2$ channel one gets

$$i\mathcal{M}_{\rm M1}^{({}^3P_2)} = -\,i\epsilon_{abc}\varepsilon_{ij}^{*}\varepsilon_c^{(\gamma)*}G_{ijalmq}p_q k_b\, h^{(2^+)}\sqrt{2M\mathcal{Z}^{(2^+)}}\,\mu_N\bigg[-\frac{[h^{(3)}]^2}{2\pi\mu}D^{(3)}(p^2/2\mu,0)\bigg]\sqrt{3}$$
$$\times\, U_N^T(-\boldsymbol{p})Q_{lm}U_C(\boldsymbol{p})\bigg[\sqrt{\frac{3}{2}}\bigg(\frac{3}{2}g_c-\frac{3}{2}g_n\bigg)I(p;\lambda)-\frac{2\pi L^{(1)}}{h^{(3)}h^{(2^+)}}\bigg]. \tag{28}$$

Numerically the gyromagnetic factors are $\sqrt{3/2}(3g_c/2+g_n/2+2\mu Z_c M_n/M_c^2)\sim 1.8$ for ${}^5P_2$ and $\sqrt{3/2}(3g_c/2-3g_n/2)\sim 11$ for ${}^3P_2$. The former is of natural size for a dimensionless constant —in Eq. (26), the two-body current dominates for a natural $L^{(2)}\sim 1$ and the loop contribution is subleading. However, the ${}^3P_2$ numerical factor is large and enhances the loop contribution beyond the estimates of the power counting. Thus in Eq. (28) the loop contribution is as important as the two-body current and both enter at leading order. For convenience, we keep the loop contribution and two-body magnetic coupling at the same order in both the spin channels. The dependence on the renormalization scale λ coming from the loop function $I(p,\lambda)$, Eqs. (26), (28), is then cancelled by the two-body couplings $L^{(1)}$ and $L^{(2)}$, respectively. We write

$$L^{(2)} = -\frac{h^{(3)}h^{(2)}}{2\pi}\bigg[\sqrt{\frac{3}{2}}\bigg(\frac{3}{2}g_c+\frac{1}{2}g_n+\frac{2\mu Z_c M_n}{M_c^2}\bigg)\lambda+\beta^{(2)}\bigg],$$
$$L^{(1)} = -\frac{h^{(3)}h^{(2)}}{2\pi}\bigg[\sqrt{\frac{3}{2}}\bigg(\frac{3}{2}g_c-\frac{3}{2}g_n\bigg)\lambda+\beta^{(1)}\bigg], \tag{29}$$

where $\beta^{(i)}$'s are renormalized two-body parameters with dimensions of mass. The total cross section can be written as

$$\sigma_{\rm M1}^{(2^+)} = \frac{1}{14}\frac{7}{3}\frac{\alpha\mu}{M_p^2}[h^{(2^+)}]^2\big|\mathcal{Z}^{(2^+)}\big|\frac{(p^2+[\gamma^{(2^+)}]^2)^3}{(2\mu p)^3}\bigg|\frac{p^2}{-1/a_1^{(3)}+\frac{1}{2}r_1^{(3)}p^2-ip^3}\bigg|^2$$
$$\times\bigg\{\bigg|\sqrt{\frac{2}{3}}\bigg(\frac{3}{2}g_c+\frac{1}{2}g_n+\frac{2\mu Z_c M_n}{M_c^2}\bigg)\frac{[\gamma^{(2^+)}]^3-ip^3}{[\gamma^{(2^+)}]^2+p^2}+\beta^{(2)}\bigg|^2$$
$$+\bigg|\sqrt{\frac{2}{3}}\bigg(\frac{3}{2}g_c-\frac{3}{2}g_n\bigg)\frac{[\gamma^{(2^+)}]^3-ip^3}{[\gamma^{(2^+)}]^2+p^2}+\beta^{(1)}\bigg|^2\bigg\}, \tag{30}$$

where the proton mass $M_p = 938.3$ MeV is used. We summed over the final state dimer and photon polarizations, and averaged over the initial spin states. The magnetic moment and orbital momentum weights are easy to understand if one compares with the non-relativistic quantum operator for the M1 transition, which is proportional to

$$\bigg(\frac{\mu M_n Z_c}{M_c^2}\vec{\boldsymbol{L}}+g_c\vec{\boldsymbol{S}}_C+g_n\vec{\boldsymbol{S}}_N\bigg)_z, \tag{31}$$

and its expectation value between the initial ${}^5P_3$ state and the final ${}^5P_2$ and ${}^3P_2$ states, respectively.

All the elastic scattering parameters have been determined. The final expression in Eq. (30) depends on two parameters $\beta^{(1)}$, $\beta^{(2)}$, that we fit to capture data near the resonance. The EFT couplings $(\Delta^{(3)}, h^{(3)})$ were matched to the position and width of the resonance in the ${}^5P_3$ elastic channel. The values of $\beta^{(i)}$s primarily affect the height of the cross section near the resonance, but not its position or width. If one follows the power counting naively then only the two-body currents contribute at LO, and the two $\beta^{(i)}$s are correlated. In the resummed amplitude, we find a similar behavior in our fits. Thus we use a common $\beta = \beta^{(1)} = \beta^{(2)}$. We find $\beta = 170$ MeV when we fit to data set ImhofB [32] (more consistent with the low-energy $1/v$ behavior observed experimentally) using the experimental 3^+ width. Instead, a fit to the same data set but with the 3^+ width extracted from Huang's potential model phase shift provides $\beta = 83$ MeV. Fitting to the data set ImhofA with Huang's 3^+ width give $\beta = -44$ MeV. The results are shown in Fig. 6, 7. Note that the authors assign a 20% error to the data sets ImhofA and ImhofB [32]. This means away from the resonance where the cross section is small, the errors are also small. This makes the region where the resonance contributes the most the least constraining in the fits.

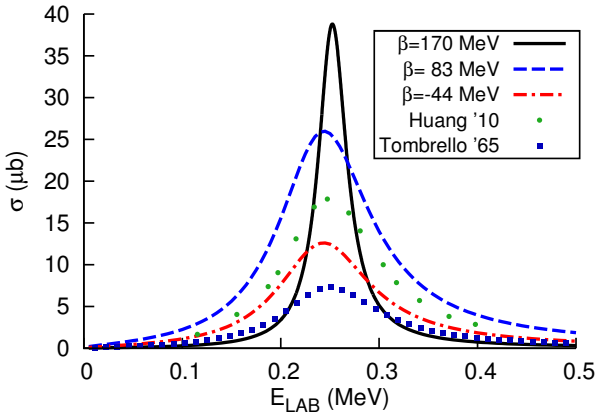

FIG. 6. M1 capture. Black curve with $\beta = 170$ MeV, resonance energy and width fitted to experimental data. Blue dashed curve with $\beta = 83$ MeV, red dot-dashed curve with $\beta = -44$ MeV, resonance energy and width fitted to Huang's potential model. Green circles are results from Huang et al., blue squares M1 capture using Tombrello's potential model in code CDXS+.

The fit with a wider resonance, $\Gamma_r = 0.11$ MeV, seems to describe the data better than

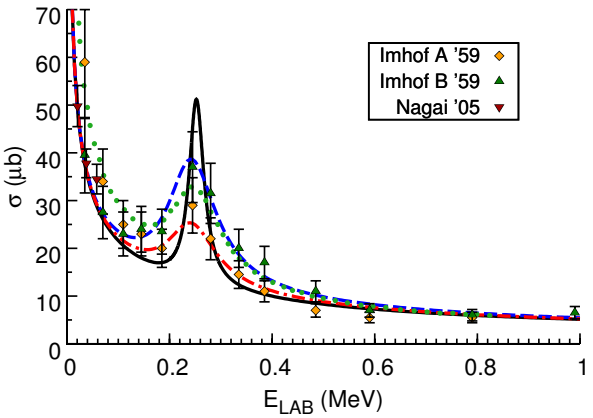

FIG. 7. Capture cross section including E1 and M1 transition. We use $r_1^{(2^+)} = -1.47$ fm^{-1}, $r_1^{(1^+)} = -1.93$ fm^{-1}. Black solid curve with $\beta = 170$ MeV and experimental resonance width, blue dashed curve $\beta = 83$ MeV, red dot-dashed curve with $\beta = -44$ MeV, and Huang's potential model resonance width. Green dots are results from Huang et al. The experimental points are from Refs. [17, 26, 32, 33].

using the experimental width $\Gamma_r = 0.031$ MeV, see Fig. 7. Smaller errorbars near the resonance than the estimated 20% ones would be useful to make stronger statements. Higher order EFT corrections estimated to be around 30% (see Appendix A) could also make the fit better even with the narrower experimental width. With these considerations in mind, we see that with the current data the LO EFT does not reproduce the width seen in the capture. This could be an indication of the limitation of the single-particle approximation to describe the capture reaction near the resonance energy as it is towards the higher momenta region of the domain of applicability of the low energy EFT. Nonetheless, the same feature is observed in the microscopic calculation of Ref. [6]. The potential models get a wider width by coincidence and it is not in agreement with the experimental value $\Gamma_r = 0.031$ MeV.

To expand the range of applicability of the EFT to slightly higher momenta, one needs to include other missing degrees of freedom. The $\frac{1}{2}^-$ excited state of the ^{7}Li core (^{7}Li*), which contributes only to the spin-1 channel, is the first to consider. It can be incorporated explicitly in the present halo EFT, since its energy remains close to the core ground state (~ 0.5 MeV) and far from the first breakup channel (~ 2.5 MeV). In the n-^{7}Li c.m. system, the energy required to probe the ^{7}Li* involves momenta of ~ 80 MeV. In the present work, the higher incoming momentum considered is ~ 40 MeV, which justifies having the ^{7}Li*

"integrated out". An analogous situation is the Delta resonance in chiral perturbation theory (the EFT for pions and nucleons) where the Delta can be integrated out of the theory when the energy relative to the pion-nucleon threshold is smaller than the nucleon-Delta mass splitting [24, 29, 34]. Further, it can also be shown that the virtual contributions of ^{7}Li* to the ground state of ^{8}Li in the neutron capture reaction is a subleading effect [35].

Contributions from d-waves to the E1 transition, which are in principle suppressed by a factor of $(Q/\Lambda)^4$, may also become relevant with increasing energy [10], depending on the desired accuracy. The next level of sophistication is the inclusion of alpha and triton degrees of freedom in a three-cluster treatment, which shall improve the description of the M1 capture reaction [7, 8].

IV. CONCLUSIONS

In the present work we extend the previous halo EFT calculation of the ^{7}Li$(n,\gamma)^8$Li capture reaction to include the complete E1 transition at leading order, as well as the leading M1 capture at low energies. We present model-independent results that quantify the current uncertainties in nuclear theory in the single-particle approximation, therefore serving as a guide to its limitations and also highlighting where more precise experimental input is necessary for improvements.

We include explicitly the E1 capture from s-waves to the excited state in ^{8}Li that contributes about 10% to the cross section at very low energy. The new EFT coupling constants associated to this process are completely determined by the binding energy of the excited state and the E1 thermal capture rate to the excited state [17]. For energies below 100 keV, our results show the expected $1/v$ behavior also seen in potential models, however, differing by a sizable overall normalization, directly related to the effective range in the ground state channel $r_1^{(2^+)}$. This is the dominant source of uncertainty in this low energy region —it could be determined from accurate elastic scattering data and partial wave analysis, but due to the present lacking of the latter it is poorly known. A fit to E1 thermal capture data gives $r_1^{(2^+)} \approx -1.47$ fm^{-1}, see also Ref. [13].

The M1 capture proceeds via the 3^+ resonance near $E \sim 0.2$ MeV in the $^5P_3$ channel. It is suppressed at very low momentum due to the p-wave initial state. However, near the resonance there is an enhanced contribution to the total cross section that needs to

be considered. In the halo EFT approach, we include and estimate the size of one-body (magnetic moment and orbital momentum couplings) and two-body currents that enters in the calculation. The one-body current contribution is consistent with the effective magnetic dipole operator used in potential models, but the two-body currents are new ingredients. These latter also renormalize loop contributions, and the corresponding couplings $\beta^{(1)}$ and $\beta^{(2)}$ are our free parameters to be determined from the capture data. The power counting for two-body currents was studied, and found to contribute at LO and N^{2}LO in the M1 and E1 capture, respectively.

The available capture data near the resonance have large errors that hampers the quality of the fit. However, given the current data near the resonance, it seems that using the experimental resonance width $\Gamma_r = 31$ keV in the 3^+ elastic amplitude does a poor job in describing the M1 capture data. This was also observed in the microscopic calculation of Ref. [6]. A significantly larger width, about three times the experimental one, provides much better fits. This is roughly the width that one gets in potential models that are tuned to the resonance energy. This is a coincidence since, in principle, one should tune the potential models to reproduce not only the resonance energy E_r but also the resonance width Γ_r accurately. In the EFT formalism, the p-wave resonance requires two operators at LO that can be fixed by matching to the resonance energy and width. The fact that halo EFT is able to describe the resonance scattering (as shown in Section II C) but not to reproduce the M1 capture might indicate the limitation of the current approach. As discussed in Section III, the M1 capture could be on the outer edge of the range of applicability. To expand this EFT range, other degrees of freedom have to be incorporated. Within the present two-body treatment, the inclusion of the $\frac{1}{2}^-$ excited state in the ^{7}Li core is the first step towards this goal. The next, more radical extension is to take the leading configuration of the ^{7}Li as a bound state of elementary alpha and triton "cores". In such a three-body approach, not only the ground and the $\frac{1}{2}^-$ excited states in ^{7}Li could be considered, but also the $\frac{7}{2}^-$ state which, according to microscopic approaches [5, 6, 8], is important to properly describe the 3^+ resonance. Nevertheless, the apparent discrepancy in the input related to the 3^+ resonance width that is used in the $^5P_3$ elastic scattering and M1 capture reaction is unlikely to be resolved with current experimental information. More precise capture data around 0.22 MeV (where the M1 capture dominates) is needed to conclusively state if the single-particle approximation is sufficient to describe the M1 capture in $^7\mathrm{Li}(n,\gamma)^8\mathrm{Li}$.

ACKNOWLEDGMENTS

We thank C. Bertulani and S. Typel for discussions and help with potential model codes RADCAP [36] and CDXS+ [31], respectively. We also thank T. Frederico, V. Guimarães, H.-W. Hammer, D. R. Phillips, S. Typel, and U. van Kolck for valuable comments and discussions. This work is partially supported by the U.S. NSF Grant No. PHY-0969378 (LF and GR), the Dutch Stichting FOM under program 114 (RH) and HPC^2 Center for Computational Sciences at Mississippi State University (GR).

Appendix A: More on Power Counting

We have seen earlier that the contribution of the two-body currents relative to the loop diagrams in M1 capture scales as $L^{(i)}/(g_{[i]}Qh^{(3)}h^{(2)})$, where $g_{[i]}$ is a combination of the gyromagnetic ratios g_c, g_n that is of natural size in the ${}^5P_2$ channel but large in the ${}^3P_2$ channel. To estimate the size of two-body currents we also need estimates for $h^{(\eta)}$ that is related to the effective range. In this section we present the details of the power counting starting with the p-wave elastic channel. This also allows one to estimate the expansion parameter Q/Λ.

In Sec. II we have fitted the ERE parameters $a_1^{(\eta)}$, $r_1^{(\eta)}$ in their respective p-channels. We found $\left|1/a_1^{(\eta)}\right|^{1/3} \sim 30 - 50$ MeV and $r_1^{(\eta)}/2 \sim 100 - 250$ MeV. This is consistent with the situation in Ref. [20], where only $1/a_1^{(\eta)}$ is fine-tuned to scale as ΛQ^2 while $r_1^{(\eta)} \sim \Lambda$ obeys the naive expectation. Then in the EFT matching conditions, Eq. (12),

$$
\begin{aligned}
-\frac{\pi}{[h^{(\eta)}]^2} &= \frac{1}{2}r_1^{(\eta)} + \frac{3}{2}\lambda, \\
-\frac{2\pi\mu\Delta^{(\eta)}}{[h^{(\eta)}]^2} &= -1/a_1^{(\eta)} + \frac{\pi}{2}\lambda^3,
\end{aligned}
$$

the renormalization scale $\lambda \sim Q$ from the loop momentum is a higher order contribution in a Q/Λ expansion. We get $[h^{(\eta)}]^2 = -2\pi/r_1^{(\eta)} \sim 1/\Lambda$ and $\mu\Delta^{(\eta)} = -1/(r_1^{(\eta)}a_1^{(\eta)}) \sim Q^2$. We expand the dimer propagator as

$$
D(p_0, \boldsymbol{p}) = D_{-2}(p_0, \boldsymbol{p}) + D_{-1}(p_0, \boldsymbol{p}) + \cdots , \tag{A1}
$$

and the LO term is given by the bare propagator,

$$
D_{-2}(p_0, \boldsymbol{p}) = \frac{1}{\Delta - \zeta^2/(2\mu)},
$$

since loop contributions enter at higher orders. The subscript indicates the scaling with powers of Q and we have suppressed the superscript η here and in the rest of this section. To renormalize the loop expansion systematically we write the couplings as [22, 37]

$$\begin{aligned} h =& h_0 + h_1 + \cdots , \\ \Delta =& \Delta_2 + \Delta_3 + \cdots , \end{aligned} \tag{A2}$$

stressing again that the subscripts bookkeep the powers in Q. Matching to the ERE we get

$$\begin{aligned} -\frac{\pi}{h_0^2} &= \frac{1}{2} r_1, & 2\pi \frac{h_1}{h_0^3} &= \frac{3}{2}\lambda, \\ \Delta_2 &= -\frac{1}{\mu r_1 a_1}, & \Delta_3 &= \frac{\pi}{2\mu r_1}\lambda^3 + \frac{3}{\mu r_1^2 a_1}\lambda. \end{aligned} \tag{A3}$$

At next-to-leading order (NLO) the dimer propagator gets a contribution from the one-loop self-energy diagram,

$$\begin{aligned} D_{-1}(p_0, \boldsymbol{p}) =& [iD_{-2}(p_0, \boldsymbol{p})]^2 \Sigma(p_0, \boldsymbol{p}), \\ i\Sigma(p_0, \boldsymbol{p}) =& i\frac{2h_0^2}{\mu} f_1(p_0, \boldsymbol{p}) + i\Delta_3 = i\frac{h_0^2}{2\pi}\zeta^3 - i\frac{3h_0^2}{4\pi\mu}\lambda\zeta^2 + i\frac{h_0^2}{4\mu}\lambda^3 + i\Delta_3 \\ =& -i\frac{\zeta^3}{r_1} + i\frac{3\zeta^2\lambda}{2\mu r_1} + \frac{3\lambda}{\mu r_1^2 a_1}, \end{aligned} \tag{A4}$$

which is a λ-dependent result. However, the elastic amplitude in Eq. (10),

$$\begin{aligned} A(p) =& -h^2 \frac{p^2}{\mu^2} D(p^2/2\mu, 0) \\ \approx& -h_0^2 \frac{p^2}{\mu^2} D_{-2}(p^2/2\mu, 0) - h_0^2 \frac{p^2}{\mu^2} D_{-2}(p^2/2\mu, 0) \left[D_{-1}(p^2/2\mu, 0)/D_{-2}(p^2/2\mu, 0) + \frac{2h_1}{h_0} \right] \\ =& \frac{2\pi}{\mu} \frac{p^2}{-1/a_1 + \frac{1}{2} r_1 p^2} \left(1 + \frac{ip^3}{-1/a_1 + \frac{1}{2} r_1 p^2} \right), \end{aligned} \tag{A5}$$

is λ-independent as expected for a physical observable. This is in agreement with the expansion of the ERE amplitude up to NLO in Q/Λ. At LO the binding momentum is given by $\gamma = \sqrt{-2/(r_1 a_1)}$. The NLO term introduces a double pole which, at least formally, is suppressed in the Q/Λ expansion. To treat the bound state consistently we rewrite the p-wave ERE expansion [22, 37] as:

$$\begin{aligned} p^3 \cot\delta(p) =& \gamma^3 + \frac{1}{2} s(p^2 + \gamma^2) + \cdots , \\ -1/a_1 =& \gamma^3 + \frac{1}{2} s\gamma^2 + \cdots , \\ r_1 =& s + \cdots , \end{aligned} \tag{A6}$$

and define the EFT couplings as

$$-\frac{\pi}{h_0^2} = \frac{1}{2} r_1, \qquad 2\pi \frac{h_1}{h_0^3} = \frac{3}{2}\lambda,$$
$$\Delta_2 = \frac{\gamma^2}{2\mu}, \qquad \Delta_3 = \frac{\pi}{2\mu r_1}\lambda^3 - \frac{3\gamma^2}{2\mu r_1}\lambda + \frac{\gamma^3}{\mu r_1}. \tag{A7}$$

The amplitude is now written as

$$A(p) = \frac{2\pi}{\mu} \frac{2p^2}{r_1(\gamma + ip)(\gamma - ip)} \left[1 + 2\frac{p^2 + ip\gamma - \gamma^2}{r_1(\gamma - ip)} \right], \tag{A8}$$

where the NLO correction contributes a factor of $-3\gamma/r_1$ to the residue at the pole $p = i\gamma$ without introducing any spurious double pole. This correction to the residue at the pole is consistent with the wave function renormalization calculated earlier,

$$h^2 \mathcal{Z} = -\frac{2\pi}{3\gamma + r_1}. \tag{A9}$$

We keep the complete result instead of expanding. A convenient approach to recover the complete result at NLO without resumation is to use the so called "zed"-parameterization [38]. In this approach one would define, for example, $h_0^2 = -2\pi(\mathcal{Z} - 1)/(3\gamma)$, $h_1 = 3h_0^3\lambda/(4\pi)$ and recover, for the wave function renormalization,

$$\mathcal{Z} = 1 + (\mathcal{Z} - 1) + 0 + 0 + \cdots, \tag{A10}$$

where $\mathcal{Z} - 1 \sim Q$ is treated as a perturbation, see Ref. [38] for details. Here we will simply use the resummed result for the 2^+ bound state and the 1^+ excited state.

So far we have discussed the fine-tuning required to reproduce a shallow (p-wave) bound or virtual state. The power counting above also applies to low lying resonances. However, for these cases there is an additional fine-tuning that is purely kinematical that was discussed in Refs. [20, 24]. This second fine-tuning requires the loop contribution to be treated non-perturbatively at energies near the resonance. Since we consider energies near the resonance in our capture calculations, we resum the loop contributions in the 3^+ initial state.

Next we come back to the role of two-body currents $L/(g_{[i]}Qh^2)$ in the M1 capture. Since $h^2 \sim 1/\Lambda$ as shown above, the relative contribution for a natural two-body current scales as $\Lambda/(g_{[i]}Q)$. At LO and from the specific numerical values of $g_{[i]}$, one notices that in the ${}^5P_2$ channel only the two-body current enters, while in the ${}^3P_2$ case both two-body and one-body (magnetic moment) currents contribute. In principle, for a systematic treatment one could

write $\beta^{(2)} = \beta_0^{(2)} + \beta_1^{(2)} + \cdots$ and perform the perturbative renormalization outlined above for the ${}^5P_2$ channel, while keeping the full loop contribution in the ${}^3P_2$ channel. We verified that such a treatment satisfies the power counting estimates. As mentioned in Sec. III, we keep the loop contribution at LO in both ${}^3P_2$ and ${}^5P_2$ channels for convenience.

The scaling of two-body currents that appear in the E1 case is different than in the M1 capture. To keep the discussion fairly general, let us introduce a dimer field $\pi^{(s-\text{wave})}$ for the two initial state s-wave channels ${}^5S_2$, ${}^3S_1$. Then the relative contribution of the two-body to one-body current in the E1 capture is generically $L_{\rm E1} k_0 \mu h^{(s-\text{wave})}/[h\Delta^{(s-\text{wave})}]$, where we considered the operator $e L_{\rm E1} \phi_{ij}^\dagger E_x \pi_{yz} T_{xyzij}$ for transition from ${}^5S_2$ to ${}^5P_2$ ground state, for illustration. $h^{(s-\text{wave})} \sim h$ is the π-nucleon-core coupling and $\Delta^{(s-\text{wave})}$ the dimer propagator in the s-wave. In the power counting one either takes $\Delta^{(s-\text{wave})} \sim \Lambda$ to treat s-wave interaction as perturbative as would be the case for small natural sized scattering length (the ${}^3S_1$ channel for momenta $p \lesssim 227$ MeV) or take $\Delta^{(s-\text{wave})} \sim Q$ to treat s-wave interaction as non-perturbative as would be the case for large unnatural sized scattering length (the ${}^5S_2$ channel around $p \sim 54$ MeV). For a natural $L_{\rm E1}$ given by dimensional analysis, the relative contribution $L_{\rm E1} k_0 \mu h^{(s-\text{wave})}/[h\Delta^{(s-\text{wave})}]$ scales as either Q^2 for perturbative or as Q for non-perturbative s-wave interaction in the initial state. The former is a N^{2}LO contribution whereas the latter is a NLO contribution.

Appendix B: Normalization of states

In this work we adopt the following definitions for the nucleon and core field operators

$$\begin{aligned}
\psi_N(\boldsymbol{x}) &= \int \frac{d^3p}{(2\pi)^3} \frac{1}{\sqrt{2M_N}} \sum_s N_s(\boldsymbol{p}) U_N^{(s)}(\boldsymbol{p}) e^{i\boldsymbol{p}\cdot\boldsymbol{x}}\,, \\
&\sum_s U_N^{(s)}(\boldsymbol{p}) U_N^{(s)\,\dagger}(\boldsymbol{p}) = 2M_N \sum_s \chi^{(s)} \chi^{(s)\,\dagger} = 2M_N\, I_{2\times 2}\,, \qquad \text{(B1)} \\
\psi_C(\boldsymbol{x}) &= \int \frac{d^3p}{(2\pi)^3} \frac{1}{\sqrt{2M_C}} \sum_r C_r(\boldsymbol{p}) U_C^{(r)}(\boldsymbol{p}) e^{i\boldsymbol{p}\cdot\boldsymbol{x}}\,, \\
&\sum_r U_C^{(r)}(\boldsymbol{p}) U_C^{(r)\,\dagger}(\boldsymbol{p}) = 2M_C \sum_r \xi^{(r)} \xi^{(r)\,\dagger} = 2M_C\, I_{4\times 4}\,, \qquad \text{(B2)} \\
&\{\psi_{N,a}(\boldsymbol{x}), \psi_{N,b}^\dagger(\boldsymbol{y})\} = \{\psi_{C,a}(\boldsymbol{x}), \psi_{C,b}^\dagger(\boldsymbol{y})\} = \delta^{(3)}(\boldsymbol{x}-\boldsymbol{y})\delta_{ab}\,, \\
&\{N_a(\boldsymbol{p}), N_b^\dagger(\boldsymbol{q})\} = \{C_a(\boldsymbol{p}), C_b^\dagger(\boldsymbol{q})\} = (2\pi)^3 \delta^{(3)}(\boldsymbol{p}-\boldsymbol{q})\delta_{ab}\,.
\end{aligned}$$

$\chi^{(s)}$ and $\xi^{(r)}$ are nucleon and core spinors in the fundamental representations of spins 1/2 and 3/2, respectively. One-neutron states are defined as

$$
\begin{aligned}
&|\boldsymbol{p}, s\rangle = \sqrt{2M_N}\, N_s^\dagger(\boldsymbol{p})|0\rangle\,, \qquad \Rightarrow \qquad \langle \boldsymbol{p}, s|\boldsymbol{q}, s'\rangle = 2M_N\,(2\pi)^3\delta^{(3)}(\boldsymbol{p}-\boldsymbol{q})\delta_{ss'}\,,\\
&\psi_N(x)|\boldsymbol{p}, s\rangle = \int \frac{d^3q}{(2\pi)^3}\frac{1}{\sqrt{2M_N}}\sum_{s'} U_N^{(s')}(\boldsymbol{q})e^{i\boldsymbol{q}\cdot\boldsymbol{x}}N_{s'}(\boldsymbol{q})\,\sqrt{2M_N}\,N_s^\dagger(\boldsymbol{p})|0\rangle\\
&\qquad\qquad = \int \frac{d^3q}{(2\pi)^3}\sum_{s'} U_N^{(s')}(\boldsymbol{q})e^{i\boldsymbol{q}\cdot\boldsymbol{x}}\{N_{s'}(\boldsymbol{q}), N_s^\dagger(\boldsymbol{p})\}|0\rangle = e^{i\boldsymbol{p}\cdot\boldsymbol{x}}U_N^{(s)}(\boldsymbol{p})|0\rangle\,.
\end{aligned}
\tag{B3}
$$

Analogously for one-core states. Generalization to multi-particle states is straightforward.

1. Projection operators

For each partial wave we construct the corresponding projection operators from the relative core-nucleon velocity, the spin-1/2 Pauli matrices σ_i's, and the following spin-1/2 to spin-3/2 transition matrices

$$
S_1 = \frac{1}{\sqrt{6}}\begin{pmatrix} -\sqrt{3} & 0 & 1 & 0 \\ 0 & -1 & 0 & \sqrt{3}\end{pmatrix}, \quad S_2 = -\frac{i}{\sqrt{6}}\begin{pmatrix} \sqrt{3} & 0 & 1 & 0 \\ 0 & 1 & 0 & \sqrt{3}\end{pmatrix}, \; S_3 = \frac{2}{\sqrt{6}}\begin{pmatrix} 0 & 1 & 0 & 0 \\ 0 & 0 & 1 & 0\end{pmatrix},
\tag{B4}
$$

which satisfy

$$
S_iS_j^\dagger = \frac{2}{3}\delta_{ij} - \frac{i}{3}\epsilon_{ijk}\sigma_k\,, \qquad S_i^\dagger S_j = \frac{3}{4}\delta_{ij} - \frac{1}{6}\big\{J_i^{(3/2)}, J_j^{(3/2)}\big\} + \frac{i}{3}\epsilon_{ijk}J_k^{(3/2)}\,,
\tag{B5}
$$

where $J_i^{(3/2)}$'s are the generators of the spin-3/2. We construct the Clebsch-Gordan coefficient matrices

$$
F_i = -\frac{i\sqrt{3}}{2}\sigma_2 S_i, \qquad\qquad Q_{ij} = -\frac{i}{\sqrt{8}}\sigma_2\big(\sigma_i S_i + \sigma_j S_i\big),
\tag{B6}
$$

and define the tensors

$$
\begin{aligned}
R_{ijxy} &= \frac{1}{2}\left(\delta_{ix}\delta_{jy} + \delta_{iy}\delta_{jx} - \frac{2}{3}\delta_{ij}\delta_{xy}\right),\\
T_{xyzij} &= \frac{1}{2}\Big(\epsilon_{xzi}\delta_{yj} + \epsilon_{xzj}\delta_{yi} + \epsilon_{yzi}\delta_{xj} + \epsilon_{yzj}\delta_{xi}\Big),\\
G_{ijklmq} &= \frac{1}{6}\Big\{ -\frac{2}{5}\Big[\delta_{qm}(\delta_{il}\delta_{jk} + \delta_{jl}\delta_{ik} + \delta_{ij}\delta_{kl}) + \delta_{ql}(\delta_{im}\delta_{jk} + \delta_{jm}\delta_{ik} + \delta_{ij}\delta_{km})\\
&\quad + \delta_{lm}(\delta_{iq}\delta_{jk} + \delta_{jq}\delta_{ik} + \delta_{ij}\delta_{kq})\Big] + (\delta_{il}\delta_{jm}\delta_{kq} + \delta_{il}\delta_{jq}\delta_{km})\\
&\quad (\delta_{jl}\delta_{km}\delta_{iq} + \delta_{jl}\delta_{kq}\delta_{im}) + (\delta_{kl}\delta_{im}\delta_{jq} + \delta_{kl}\delta_{iq}\delta_{jm})\Big\},
\end{aligned}
\tag{B7}
$$

that assure the correct number of independent indices for a given total angular momentum. The latter have the following properties,

$$
\begin{aligned}
R_{ijlm} &= R_{jilm} = R_{ijml} = R_{lmij}\,, \\
T_{ijklm} &= T_{jiklm} = T_{ijkml} = -T_{lmkij}\,, \\
G_{ijklmq} &= G_{jiklmq} = G_{kjilmq} = G_{ikjlmq} = G_{ijkmlq} = G_{ijkqml} = G_{ijklqm} = G_{lmqijk}\,, \\
&\Rightarrow R_{ijxy}R_{xylm} = R_{ijlm}\,, \qquad R_{ijxy}T_{xyklm} = T_{ijkxy}R_{xylm} = T_{ijklm}\,, \\
&\quad G_{abcijk}G_{ijklmn} = G_{abclmn} = R_{abxy}G_{xyclmn}\,.
\end{aligned}
\tag{B8}
$$

We introduce the photon vector ($\varepsilon_i^{(\gamma)}$), spin-1 (ε_j), spin-2 (ε_{ij}) and spin-3 tensor (ε_{ijk}) polarizations, obeying the following sums [39],

$$
\sum_{\text{pol.}} \varepsilon_i^{(\gamma)}\varepsilon_j^{(\gamma)*} = \delta_{ij} - \frac{k_i k_j}{k^2}\,, \quad \sum_{\text{pol.avg.}} \varepsilon_i\varepsilon_j^* = \frac{\delta_{ij}}{3}\,, \quad \sum_{\text{pol.avg.}} \varepsilon_{ij}\varepsilon_{lm}^* = \frac{R_{ijlm}}{5}\,, \quad \sum_{\text{pol.avg.}} \varepsilon_{ijk}\varepsilon_{lmq}^* = \frac{G_{ijklmq}}{7}\,. \tag{B9}
$$

All these elements, together with the matrices F_i and Q_{ij} from Eq. (B6), allow us to build the operators, in coordinate space,

$$
\begin{aligned}
P_i^{(^3P_1)} &= \sqrt{\frac{3}{2}}F_x \left(\frac{\overrightarrow{\nabla}}{M_c} - \frac{\overleftarrow{\nabla}}{M_n}\right)_y \epsilon_{ixy}, \\
P_{ij}^{(^3P_2)} &= \sqrt{3}F_x \left(\frac{\overrightarrow{\nabla}}{M_c} - \frac{\overleftarrow{\nabla}}{M_n}\right)_y R_{xyij}, \\
P_i^{(^5P_1)} &= \sqrt{\frac{9}{5}}Q_{ix} \left(\frac{\overrightarrow{\nabla}}{M_c} - \frac{\overleftarrow{\nabla}}{M_n}\right)_x, \\
P_{ij}^{(^5P_2)} &= \frac{1}{\sqrt{2}}Q_{xy} \left(\frac{\overrightarrow{\nabla}}{M_c} - \frac{\overleftarrow{\nabla}}{M_n}\right)_z T_{xyzij}, \\
P_{ijk}^{(^5P_3)} &= \sqrt{3}Q_{xy} \left(\frac{\overrightarrow{\nabla}}{M_c} - \frac{\overleftarrow{\nabla}}{M_n}\right)_z G_{ijkxyz},
\end{aligned}
\tag{B10}
$$

or in the momentum space,

$$
\begin{aligned}
\hat{P}_j^{(^3S_1)} &= F_j\,, \\
\hat{P}_{ij}^{(^5S_2)} &= Q_{ij}\,, \\
\tilde{P}_j^{(^3P_1)} &= \bar{p}_z\, i\sqrt{\frac{3}{2}}\, F_y \epsilon_{jyz} = \bar{p}\, i\sqrt{\frac{3}{2}}\, F_y\, \frac{\bar{p}_z}{\bar{p}}\, \epsilon_{jyz} = \bar{p}\, \hat{P}_j^{(^3P_1)}\,, \\
\tilde{P}_j^{(^5P_1)} &= \bar{p}_z\, i\frac{3}{\sqrt{5}}\, Q_{jz} = \bar{p}\, i\frac{3}{\sqrt{5}}\, \frac{\bar{p}_z}{\bar{p}}\, Q_{jz} = \bar{p}\, \hat{P}_j^{(^5P_1)}\,, \\
\tilde{P}_{ij}^{(^3P_2)} &= \bar{p}_z\, i\sqrt{3} F_y R_{yzij} = \bar{p}\, i\sqrt{3} F_y\, \frac{\bar{p}_z}{\bar{p}}\, R_{yzij} = \bar{p}\, \hat{P}_{ij}^{(^3P_2)}\,, \\
\tilde{P}_{ij}^{(^5P_2)} &= \bar{p}_z\, \frac{i}{\sqrt{2}}\, Q_{xy} T_{xyzij} = \bar{p}\, \frac{i}{\sqrt{2}}\, Q_{xy}\, \frac{\bar{p}_z}{\bar{p}}\, T_{xyzij} = \bar{p}\, \hat{P}_{ij}^{(^5P_2)}\,, \\
\tilde{P}_{ijk}^{(^5P_3)} &= \bar{p}_z\, i\sqrt{3}\, Q_{xy} G_{xyzijk} = \bar{p}\, i\sqrt{3}\, Q_{xy}\, \frac{\bar{p}_z}{\bar{p}}\, G_{xyzijk} = \bar{p}\, \hat{P}_{ijk}^{(^5P_3)}\,,
\end{aligned}
\tag{B11}
$$

where we used

$$
\mu = \frac{M_C M_N}{M_C + M_N}\,, \qquad r = \frac{M_C - M_N}{M_C + M_N}\,, \qquad \bar{p} = p^- - r p^+ = \frac{p_c - p_n}{2} - r\, \frac{p_c + p_n}{2}\,. \tag{B12}
$$

The projector operators, defined by

$$
\mathcal{P}^{(\eta)} = \hat{P}^{(\eta)}_{[i]} \varepsilon_{[i]} \tag{B13}
$$

where $[i]$ representing collectively the indices in a given channel, satisfy

$$
\sum_{\text{pol.avg.}} \mathrm{Tr}\big[\mathcal{P}^{(\eta)} \mathcal{P}^{(\eta)\dagger}\big] = 1\,. \tag{B14}
$$

This can be straightforwardly verified from the relations above and

$$
\mathrm{Tr}[F_i F_j^\dagger] = \delta_{ij}\,, \qquad \mathrm{Tr}[Q_{ij} Q_{lm}^\dagger] = R_{ijlm}\,. \tag{B15}
$$

---

[1] C. Bertulani and A. Gade, Phys.Rept., **485**, 195 (2010), arXiv:0909.5693 [nucl-th].

[2] T. Rauscher, Int.J.Mod.Phys., **E20**, 1071 (2011), arXiv:1010.4283 [nucl-th].

[3] C. Bertulani, Z. Phys. A, **356**, 293 (1996).

[4] P. Navratil, C. Bertulani, and E. Caurier, Phys.Lett., **B634**, 191 (2006), arXiv:nucl-th/0511029 [nucl-th]; Phys.Rev., **C73**, 065801 (2006), arXiv:nucl-th/0601019 [nucl-th].

[5] P. Navratil, R. Roth, and S. Quaglioni, Phys.Rev., **C82**, 034609 (2010), arXiv:1007.0525 [nucl-th].

[6] K. Bennaceur, F. Nowacki, J. Okolowicz, and M. Ploszajczak, Nucl.Phys., **A651**, 289 (1999), arXiv:nucl-th/9901060 [nucl-th].

[7] N. B. Shul'gina, B. V. Danilin, V. D. Efros, J. M. Bang, J. S. Vaagen, and M. V. Zhukov, Nuclear Physics A, **597**, 197 (1996), ISSN 0375-9474; L. Grigorenko, B. Danilin, V. Efros, N. Shul'gina, and M. Zhukov, Phys.Rev., **C60**, 044312 (1999).

[8] P. Descouvemont and D. Baye, Nuclear Physics A, **567**, 341 (1994), ISSN 0375-9474; P. Descouvemont, Phys.Rev., **C70**, 065802 (2004).

[9] T. Tombrello, Nucl. Phys., **71**, 459 (1965).

[10] B. Davids and S. Typel, Phys. Rev. C, **68**, 045802 (2003).

[11] J. T. Huang, C. A. Bertulani, and V. Guimaraes, At. Data Nuc. Data Tables, **96**, 824 (2010).

[12] L. H. Kawano, W. A. Fowler, R. W. Kavanagh, and R. A. Malaney, Astrophys. J., **372**, 1 (1991).

[13] G. Rupak and R. Higa, Phys.Rev.Lett., **106**, 222501 (2011), arXiv:1101.0207 [nucl-th].

[14] S. Typel and G. Baur, Nucl. Phys., **A759**, 247 (2005).

[15] D. R. Phillips and H. W. Hammer, EPJ Web Conf., **3**, 06002 (2010); H.-W. Hammer and D. Phillips, Nucl.Phys., **A865**, 17 (2011), arXiv:1103.1087 [nucl-th].

[16] L. Trache *et al.*, Phys. Rev. C, **67**, 062801 (2003).

[17] J. E. Lynn, E. T. Jurney, and S. Raman, Phys. Rev. C, **44**, 764 (1991).

[18] L. Koester, K. Knopf, and W. Waschkowski, Z. Phys., **A312**, 81 (1983); C. Angulo *et al.*, Nucl. Phys., **A716**, 211 (2003).

[19] C. A. Bertulani, H. W. Hammer, and U. Van Kolck, Nucl. Phys., **A712**, 37 (2002).

[20] P. F. Bedaque, H. W. Hammer, and U. van Kolck, Phys. Lett., **B569**, 159 (2003).

[21] N. J. Stone, At. Data Nuc. Data Tables, **96**, 75 (2005).

[22] J.-W. Chen, G. Rupak, and M. J. Savage, Nucl. Phys., **A653**, 386 (1999).

[23] D. B. Kaplan, M. J. Savage, and M. B. Wise, Phys. Lett., **B424**, 390 (1998); M. C. Birse, J. A. McGovern, and K. G. Richardson, Phys.Lett., **B464**, 169 (1999), arXiv:hep-ph/9807302 [hep-ph]; J. Gegelia, **B429**, 227 (1998); U. van Kolck, (1997), arXiv:hep-ph/9711222 [hep-ph]; Nucl.Phys., **A645**, 273 (1999), arXiv:nucl-th/9808007 [nucl-th].

[24] V. Pascalutsa and D. R. Phillips, Phys.Rev., **C67**, 055202 (2003), arXiv:nucl-th/0212024 [nucl-th].

[25] F. C. Barker, Nucl. Phys., **A588**, 693 (1995).

[26] J. C. Blackmon *et al.*, Phys. Rev. C, **54**, 383 (1996).

[27] J. J. Sakurai, *Modern Quantum Mechanics* (Addison Wesley Longman, New York, 1994).

[28] R. Higa, H.-W. Hammer, and U. van Kolck, Nucl.Phys., **A809**, 171 (2008), arXiv:0802.3426 [nucl-th]; B. A. Gelman, Phys.Rev., **C80**, 034005 (2009), arXiv:0906.5502 [nucl-th].

[29] B. Long and U. van Kolck, Nucl.Phys., **A840**, 39 (2010), arXiv:0907.4569 [hep-ph].

[30] H. W. Hammer and D. Lee, Phys. Lett., **B681**, 500 (2009); Annals Phys., **325**, 2212 (2010).

[31] S. Typel, Private communication.

[32] W. L. Imhof, R. G. Johnson, F. J. Vaughn, and M. Walt, Phys. Rev., **114**, 1037 (1959), the two data sets correspond to two different normalizations of the same data.

[33] Y. Nagai *et al.*, Phys. Rev. C, **71**, 055803 (2005).

[34] T. D. Cohen, B. A. Gelman, and U. van Kolck, Phys.Lett., **B588**, 57 (2004), arXiv:nucl-th/0402054 [nucl-th].

[35] R. Higa and G. Rupak, in preparation.

[36] C. A. Bertulani, Computer Physics Communications, **156**, 123 (2003).

[37] G. Rupak and N. Shoresh, Phys. Rev., **C60**, 054004 (1999), arXiv:nucl-th/9902077.

[38] D. R. Phillips, G. Rupak, and M. J. Savage, Phys. Lett., **B473**, 209 (2000), arXiv:nucl-th/9908054.

[39] S. Choi, J. Lee, J. S. Shim, and H. Song, J. Korean Phys. Soc., **25**, 576 (1992); S. Fleming, T. Mehen, and I. W. Stewart, Nucl. Phys., **A677**, 313 (2000).